Journal of optoelectronics and Advanced Materials Vol. 7, No. 5, October 2005, p. 2743 - 2752

DIELECTRIC PROPERTIES OF MOLYBDENUM OXIDE THIN FILMS

Esmat Abdel-fattah I. Saad*

Department of Engineering Physics and Mathematics, Faculty of Engineering,
Ain Shams University, Cairo, Egypt

AC coductivity measurements of Molybdenum Oxide thin films (MoO_3) are investigated within the frequency range 10^2-2.5×10^5 Hz and the temperature range of 273 – 393 K. The frequency dependence of the impedance measurements plotted in the complex plane reveals three semicircular arcs. The system could be represented by an equivalent circuit of a bulk resistance in series with three parallel resistance-capacitance combinations corresponding to contributions from the grain-bulk, grain-boundary, and electrode–film regions. The dielectric constant ε' increases with temperature and decreases with frequency, whereas the dielectric loss ε'' displays a broad maximum peak whose position shifts with temperature to a higher frequency region. The Cole – Cole diagrams of the relation ε'' (ε') show also three semicircular arcs, where some regions dominate the others. The temperature-dependence of, both the molecular relaxation time τ and dc conductivity σ, yield for the first time, three lines with different activation energies. The optical dielectric constant ε'_∞ was also separated to three curves, which increase with temperature to give broad peaks at ~341K.

(Received May 31, 2005; accepted September 22, 2005)

Keywords: Molybdenum oxide, Thin films, Dielectric properties, Relaxation time, Grain-bulk, Grain-boundary, Electrode–film, Impedanc measurements

1. Introduction

Thin films of metal–oxide insulator compounds are used in a wide range of applications, such as manufacturing semiconductor devices, e.g. transistors, and integrated circuits. In metal–oxide compounds, like molybdenum oxide (MoO_3), thin films are difficult to be prepared by thermal evaporation process, bacause of decomposition and the prefrential evaporation of the lower–vapor pressure of the constituent atoms. In metal–oxide compounds, the metallic constituent usually has the lower–vapor pressure [1]. Thus, these evaporated films may often contain an excess of metal atoms, which can act as donor or doping centers [2]. It requiers only one molecule per million to yield an impurity level of the order 10^{17} cm^{-3} [1,2]. It was suggested that, this dopant controls the electrical properties of the films, and so the energy diagram of the dopant films will be different from that of the undopant ones.

Molybdenum oxide thin films (MoO_3) have their optical absorption peak close to the human eye snsitivity peak [3,4]. This property makes MoO_3 thin films very attractive for applications in optoelectronic devices [5]. These compounds show photochromic [6,7], electrochromic [4,8-11], and thermochromic [12] effects, which make them very important for smart windows and display applications.

Since molybdenum oxide thin films are n–type semiconducting oxide [1,2,13], its resistance is affected by the presence of gases. So, MoO_3 thin films have been extensively used for detecting a variety of gases, like ammonia, CO, NO, and NO_2 [13, 14].

Complex impedance specroscopy is a flexible tool for simultaneous electrical and dielectrical characterization of materials. This powerful technique has been widely used to characterize the dielectric behavior of single crystal [15,16], polycrystalline [17,18], and amorphous materials [19,20]. AC impedance analysis allows us to inspect various phenomena occuring in the specimen under different conditions. The most important advantage of AC measurements is that,

* Corresponding author: esafisaad@yahoo.com

they can distinguish individual contributions to conductivity or polarization from different sources. In the case of polycrystalline materials, where trapping charges play an important role, the material may be divided into three regions, the grain–bulk (or lattice), the grain–boundaries, and the electrode–film interface (or contact–surface) regions [21,22].

In the present work, we report our investigations for complex dielectric properties of molybdenum oxide (MoO_3). The dielectric measurements have been performed on thin films, using the so-called Cole-Cole plots [23], as a function of temperature.

2. Experimental procedure

The samples were fabricated on glass substrates by vacuum deposition of successive layers of gold, molybdenum oxide, and gold, without breaking vacuum. The first gold electrode was evaporated at a pressure of $\sim 10^{-5}$ Torr. Molybdenum oxide was then deposited on to the gold film at a rate of deposition of 10 Å/s. The oxygen having been leaked into the system, during evaporation process with a pressure of 9×10^{-4} Torr. Glass substrates were maintained at 400 K during evaporation process. Thickness of molybdenum oxide films ranged between 3000–6000 Å, while effective area were 20–25 mm^2. The oxygen pressure, substrate temperature (T>375 K), and molybdenum oxide deposition rate, give the stable structure of molybdenum oxide thin films, α–MoO_3 [2,24].

To investigate the dielectric constant, dielectric loss and impedance, a DSP Lock-in amplifier (Signal Recovery) model 7265, was used. The sample was placed in a chamber evacuated to about 10^{-3} Torr, specially designed to minimize both stray capacitance and ambient gases effects. The range of frequencies was 10^2 – 2.5×10^5 Hz. The temperature of the sample was measured by a calibrated K-type thermocouple over a temperature range 273 – 393 K. The thermocouple was connected in series with an automatic rellay and a digital temperature indicator which allowed controlling the temperature automatically to ± 1K.

3. Results and discussion

Complex impedance behavior can be described by a series of tripple parallel R-C circuit elements, that corresponds to the dielectric behavior of the grain-bulk, the grain-boundary, and the electrode-film, respectively. These are characterized by the parameters, (R_g ,C_g), (R_{gb},C_{gb}), and (R_e, C_e), where R resembles the resistance, and the capacitance C resembles the polarization of these regions. The grain-bulk impedance arises from the lattice bulk of the thin film, while the grain-boundary impedance originates from the trapped charges, due to impurities or defects in the sample [21]. The grain-boundary is suggested to be a continuous phase, or a blocking layer of high resistivity, surrounding the grain-bulk region [25]. As for the electrode-film impedance, it comes from the contribution from migration effects. Ionic species or charges can diffuse towards the electrode-film contact and accumulate there [26].

Fig. 1. Shows, schematically, a complex impedance diagram, in which Z″ is plotted against Z′, where Z′ and Z″ are the real and imaginary parts of the complex impedance Z*.

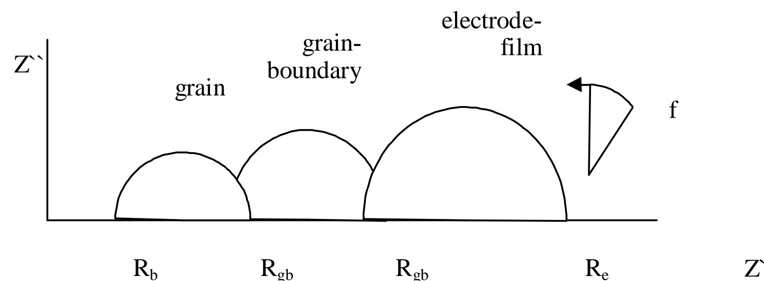

Fig. 1. Schematic diagram of complex impedance spectra showing arcs due to three regions. Arrow direction shows increasing frequency.

A more satisfactory approach may be taken by considering a simple equivalent circuit. Fig. 2 shows an idealized equivalent circuit, that gives rise to the three arcs shown in Fig.1. A resistance R_b is added, in series, to the parallel capacitance-resistance combinations, to represent the contribution to resistance from the grain-bulk interior. The grain-boundary normally exhibits higher resietance than the grain-bulk, and lower resistance than the electrode-film. So,

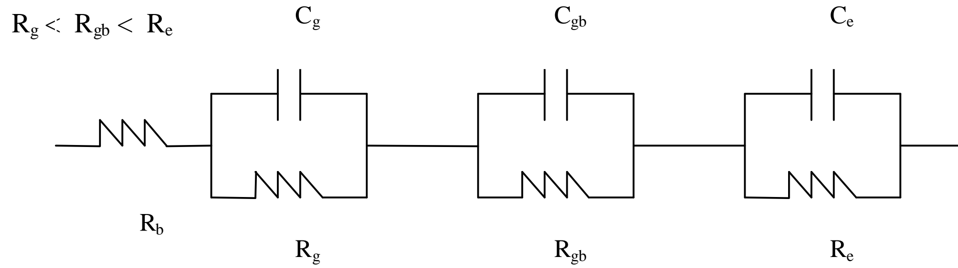

Fig. 2. The equivalent circuit corresponding to the three regions of Fig. 1.

The complex impedance, Z*, of this circuit can be written as,

$$Z^* = Z' - i\,Z'' \tag{1}$$

And, the complex dielectric constant can be written as,

$$\varepsilon^* = \varepsilon' - i\,\varepsilon'' \tag{2}$$

where, ε', and ε'', are the real and imaginary parts of the complex dielectric constant.

The dissipation factor or loss tangent, tan δ, is often used to characterize the dielectric loss of a material, which is given by

$$\tan\delta = Z'' / Z' = \varepsilon'' / \varepsilon' \tag{3}$$

where the dielectric constant ε' is given by the relation C/C_o, where C is the measured capacitance, and C_o is the geometrical capacitance, which is given for a film by the vacuum permittivity ε_o , area A and thickness t in the relation, $C_o = \varepsilon_o A / t$.

For Z′ and Z″, we have, where $i = \sqrt{-1}$, ω is the angular frequency (=2πf),

$$Z' = R_b + \frac{R_g}{1+(\omega R_g C_g)^2} + \frac{R_{gb}}{1+(\omega R_{gb} C_{gb})^2} + \frac{R_e}{1+(\omega R_e C_e)^2} \tag{4}$$

and,

$$Z'' = \frac{\omega R_g^2 C_g}{1+(\omega R_g C_g)^2} + \frac{\omega R_{gb}^2 C_{gb}}{1+(\omega R_{gb} C_{gb})^2} + \frac{\omega R_e^2 C_e}{1+(\omega R_e C_e)^2} \tag{5}$$

Figs. 3 and 4 show the variation of the real and imaginary parts, Z′ and Z″, of the complex impedance, as a function of frequency, at various temperatures. Z′ decreases as the frequency and temperature increase. The curves show two broad maxima between 600 Hz $< f <$ 3600 Hz, at $T < 293$ K. These maxima disappear at $T \geq 293$ K. At low and high frequencies, for $T \geq 293$ K, Z′ does not show appreciable change due to the change of temperature. As for the imaginary part Z″, we can see that, the curves display broad peaks. The position of the peak maximum shifts, towards higher frequencies, with increasing temperature.

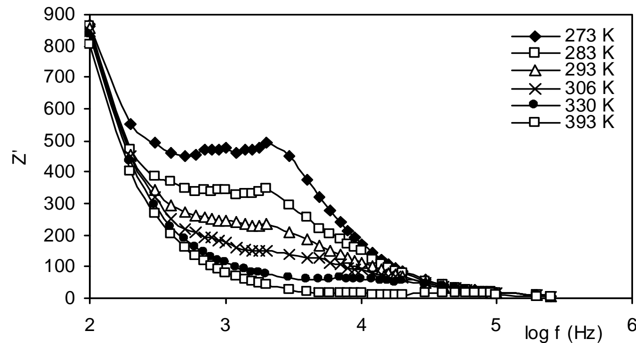

Fig. 3. Relation between Z' and log f.

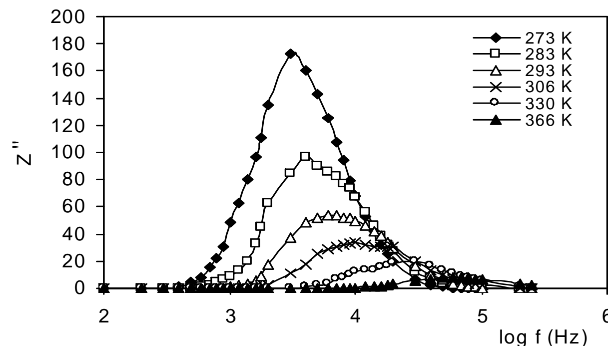

Fig. 4. Relation between Z'' and log f.

The imaginary part of the electrical impedance Z″ was plotted versus its real part Z′ for various temperatures. Typical complex impedance spectra of MoO_3 thin films, related to the applied frequency for various temperatures, are shown in Fig.5. Through the whole range of measurements, the Cole –Cole plots reveal three crossing semicircular arcs. The analysis of these semicircular arcs gives, from the high frequency side, the grain-bulk, the grain-boundary, and at last, the electrode-film impedance at the low frequency side. All these semicircles are not perfect semicircles, but inclined with their centers below the Z'-axis by an angle, which is different for each case.

At low temperatures, < 306 K, the grain-boundary impedance dominates both the grain-bulk, and the electrode-film impedances. When the temperature increases, ≥ 306 K, the grain-bulk dominates both the grain-boundary and the electrode-film, until T = 341 K, where the grain-boundary becomes comparable to the grain-bulk, and both dominate the electrode-film region. At T>341 K, the grain-bulk region dominates again until T≥378 K, where the grain-bulk region and grain-boundary become comparable, and again both dominate the electrode-film region.

In Fig.5, Z″ vanishes upon approaching both the lowest and highest frequencies, for each region, whereas Z′ varies throughout the applied frequency. Therefore, the complex impedance diagram Z″(Z′) would reflect R_b at higher frequencies, whereas contribution of R_g, R_{gb}, and R_e, increases upon shifting to the lower frequencies. The intersection of the real axis with the lower-frequency extrapolation of the three semicircles gives R_g, R_{gb}, and R_e,.

In Fig. 5, it is seen that, as the temperature increases, the impedance of the three regions decreases and moves towards lower values. We can observe, that the grain-bulk resistance, R_g, the grain-boundary resistance, R_{gb}, and the electrode-film resistance, R_e, are temperature- dependent and decrease as the temperature increases. The temperature dependence of a resistance R, is represented via a thermally – activated process, with the formula

$$R = R_o \exp. (\Delta E / k T) \tag{6}$$

where R_o is a constant, and ΔE the activation energy. The extrapolated resistances at the lower frequencies, R_g, R_{gb}, and R_e, could be used to evaluate the coductivity, using the formula,

$$\sigma_{DC} = \sigma_o \exp. (- \Delta E / kT) \tag{7}$$

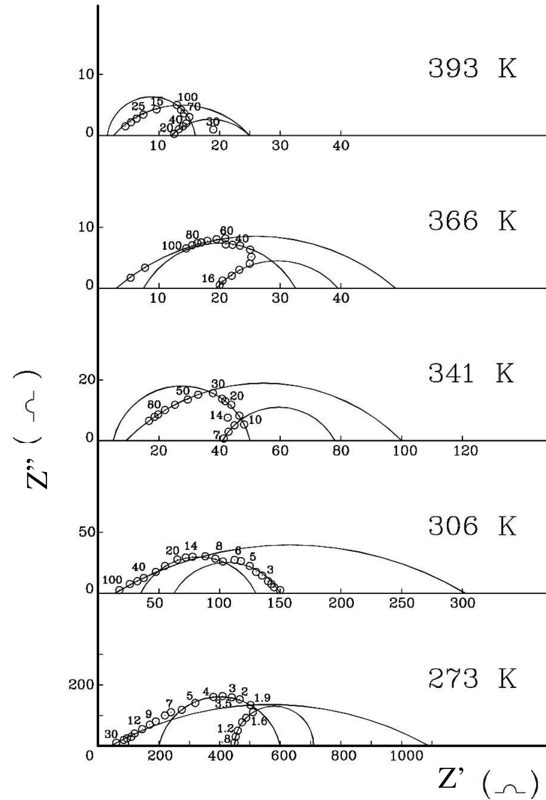

Fig. 5. Complex impedance spectra of MoO_3 for a range of temperature. The frequencies are in kHz.

Fig. 6 shows the variation of log σ_{DC} of the three regions of the sample of MoO_3, versus 1/T. The slope of each curve gives the activation energy for each region. ΔE = 0.289 eV, 0.249 eV, and 0.226 eV, while σ_o = 1.318, 0.955, and 0.724 Sm^{-1}, for the grain-bulk, grain-boundary, and electrode-film regions respectively. Only, one value, for the activation energy was given by ref. [2], for the measured values of conductance versus 1/T, to be 0.274 eV, and for frequency versus 1/T to be 0.272 eV. The mean value of our results gives ΔE = 0.255 eV. We can see for DC conductivity, that $\Delta E_g > \Delta E_{gb} > \Delta E_e$.

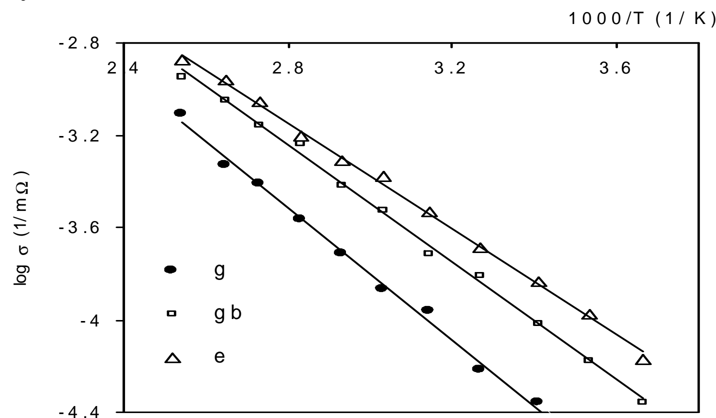

Fig. 6. Variation of σ (dc) versus 1000/T.

Figs. 7 and 8, show the frequency-dependence of the dielectric constant ε′ and dielectric loss ε″ at different temperatures. The dielectric constant ε′ decreases with increasing frequency, and increases with increasing temperature. As for the dielectric loss ε″, all the curves increase to a maximum value to give a broad peak, and then decrease to lower values. The position of the peak–

maximum shifts towards higher frequencies as the temperature increases. The peaks hight increases to a maximum value at T = 306 K, and then decreases to a lower value at T = 341 K, after which it increases again to another maximum value at T = 366 K, and then decreases again.

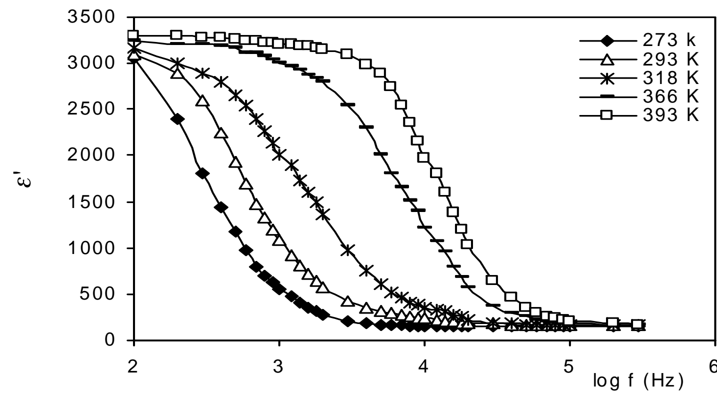

Fig. 7. Relation between ε' and log f.

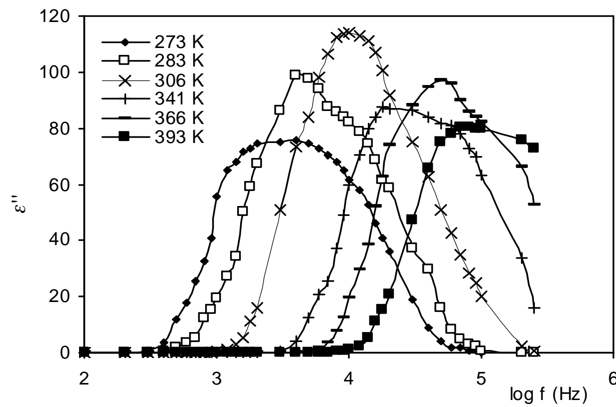

Fig. 8. Relation between ε'' and log f.

Figs. 9, and 10, show the temperature-dependence of the dielectric constant ε′, and dielectric loss **ε″,** of MoO_3 thin films (at constant frequencies). The dielectric constant ε′ increases slowly until 306 - 310 K, afterwhich it increases progressively to yield higher values. As for the dielectric loss ε″, it increases to a maximum value, afterwhich it goes to a lower value. The peak maxima are nearly between 306 - 310 K.

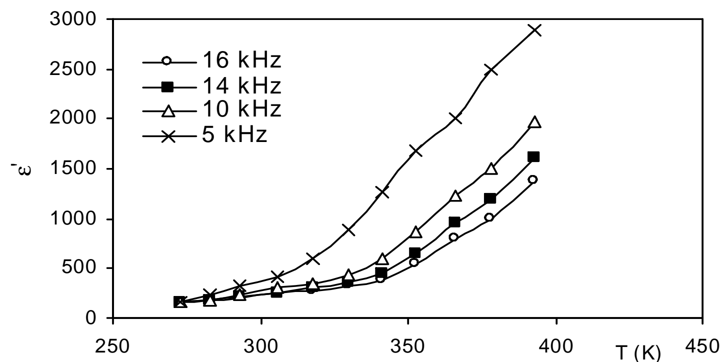

Fig. 9. Temperature-dependence of ε'.

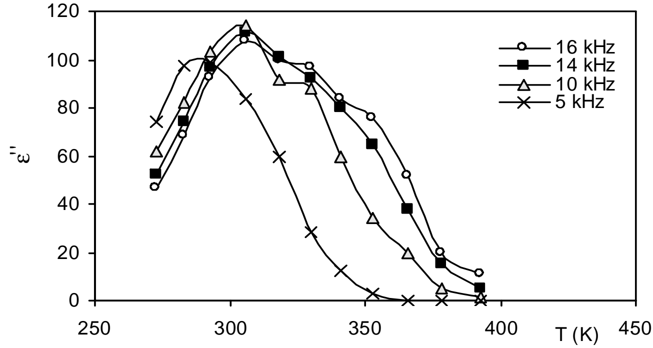

Fig. 10. Temperature – dependence of ε''.

The Cole-Cole diagrams ε″ (ε′) for MoO_3 thin films are shown at several temperatures in Fig.11. Three semisircular arcs are obtained for each temperature. The centers of the semisircles lie below the abscissa axes by an angle α, which is different for each case. This confirms that there exists a distribution of relaxation times in MoO_3 thin films. The points, at higher frequencies, which do not belong to the grain-bulk arc, are due to stray capacitance. This stray capacitance disappears at higher temperatures. The analysis of the results could reveal several parameters, such as the macroscopic relaxation time τ_o, the molecular relaxation time τ, the activation energy for relaxation E_o , and the distribution parameter α [23, 27, 28].

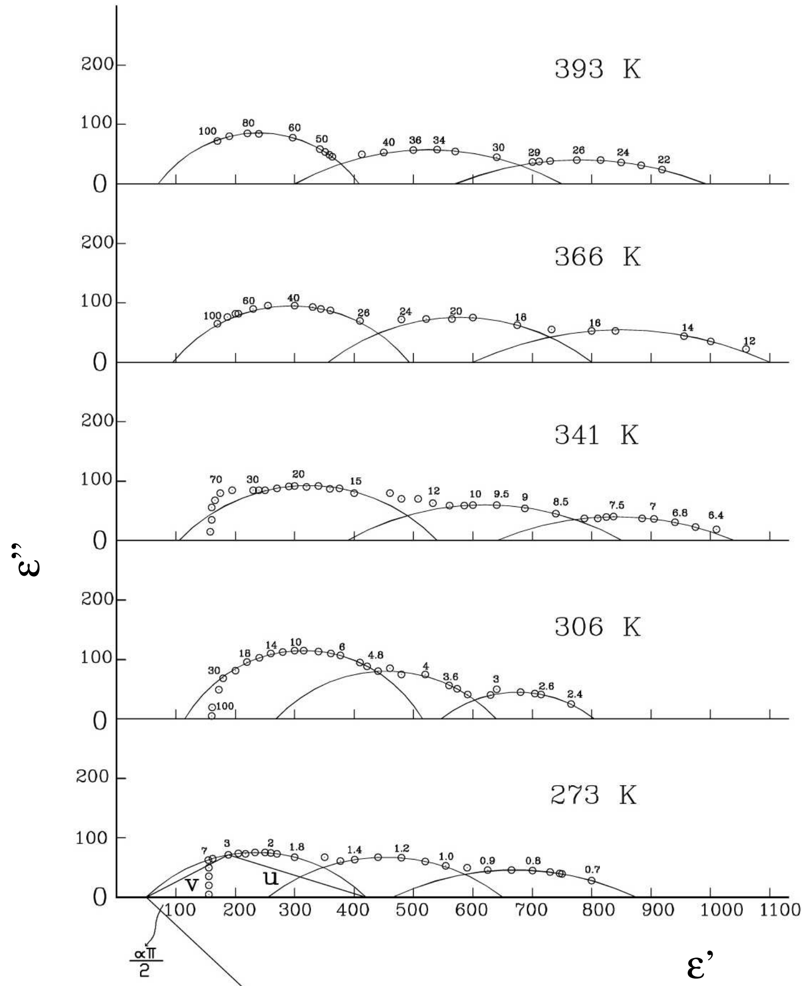

Fig. 11. The Cole – Cole diagrams of MoO_3 for a range of temperatures. The frequencies are kHz.

The macroscopic relaxation time τ_o can be evaluated using the relation [23]

$$\frac{U}{V} = (\omega \tau_o)^{1-\alpha} \tag{8}$$

where U is the distsnce on the Cole-Cole diagram between the static dielectric constant ε'_o and the experimental point, V is the distance between that point and the optical dielectric constant ε'_∞, and ω is the angular frequency. The symbols α, U, and V are shown in Fig.11. The extent of the distribution of relaxation times increases with increasing values of the parameter α , while the value of τ_o was found to decrease with temperature.

The molecular relaxation time τ could be evaluated from [28],

$$\tau = \frac{2\varepsilon'_o + \varepsilon'_\infty}{3\varepsilon'_o}\tau_o \tag{9}$$

The temperature dependence of τ is a thermally activated process, described by the relation [29–32],

$$\tau = \tau_\infty \exp(E_o / kT) \tag{10}$$

where τ_∞ is the relaxation time at infinite temperature. It represents the time of a single oscillation of a dipole in the potential well, E_o is the activation energy for relaxation, while τ represenrs the average or most probable value of a spread of relaxation times.

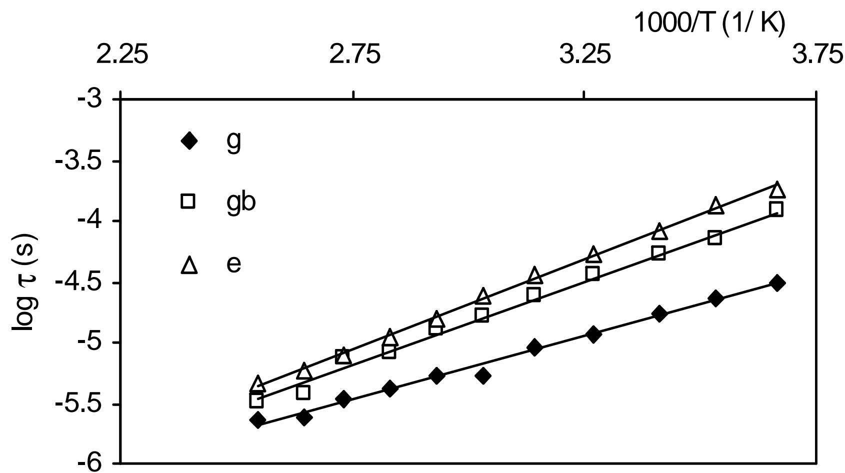

Fig. 12. Relation between log τ and 1/T.

Fig.12 shows the relaxation time τ for MoO_3 thin films, plotted against the reciprocal of temperature for the three regions. Fig.12 clearly shows three linear relations between ln τ and 1/T. The calculated values of τ_∞ and E_o were found to be 1.995×10^{-9} s, 0.21 eV, 4.467×10^{-9} s, 0.27 eV, and 5.495 $\times10^{-10}$ s, 0.31 eV, for the grain bulk, grain-boundary and electrode-film regions, respectively. The mean value of our results gives E_o= 0.264 eV , higher than the value obtained from our dc conductivity, but comparable to the value (0.272 eV) obtained by ref [2] for AC measurements. The lower value of dc activation energy may be due to oxygen vacancies and other defects, which may decrease the band gap [3,7]. It is seen from Fig. 12, that for the relaxation times, $\tau_{\text{electrode-film}} > \tau_{\text{grain-boundary}} > \tau_{\text{grain bulk}}$, and for the activation energies, $E_{o\ \text{electrode-film}} > E_{o\ \text{grain-boundary}} > E_{o\ \text{grain bulk}}$.

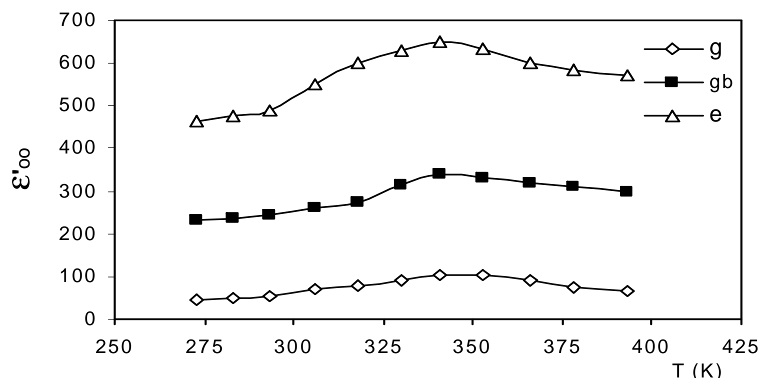

Fig. 13. Variation of ε_{oo} with Temperature.

The variation of the optical dielectric constant ε'_∞ with temperature, calculated from Fig. 11, is represented in Fig. 13. It is seen from fig. 13, that ε'_∞ increases with temperature to yield a broad maximum at ~341 K, for the grain-bulk, grain-boundary, and electrode-film regions. At T~341 K, the dielectric loss ε" is minimum, which gives a maximam value for the dielectric constant, since both are sharing together to the complex dielectric constant.

4. Summary and conclusion

The impedance spectra of molybdenum oxide (MoO_3) thin films, in the frequency range 10^2-$2.5x10^5$ Hz, and within the temperature range 273-393 K, have been investigated. The Cole-Cole plots yield three esmicircular arcs, arising from the contribution of the grain-bulk, grain-boundary, and electrode-film regions of the film. At temperature of 306 K ≤ T< 341 K, the grain-bulk region dominates both the grain-boundary and the electrode-film regions. Both the temperature-dependence relations of σ_{dc} and τ allowed to separate the three regions, giving rise to three lines with different activation energies. At T~341 K, the dielectric loss ε" is minimum, and so, the optical dielectric constant ε'_∞ for the three separated regions yields a maximum peak at this temperature.

To our knowledge, it is the first time, that the three regions of the grain bulk, grain-boundary and electrode-film are separated, in the relations of σ_{dc}-temperature and τ-temperature, where three lines were found, each with different activation energy. Also, in the relation ε'_∞ - temperature, three separated different curves, due to the three regions, were obtained. The separation of the three regions helps us to find the individual properties of each region.

Acknowledgment

The author would like to thank Prof.Dr. Abdel-Halim Zekri, at the Faculty of Engineering, Ain Shams University, Cairo, Egypt, for many informative discussion and his encouragement during this work.

References

[1] J. G. Simmons, Phys. Rev. **166**, 912 (1968).
[2] G. S. Nadkarni, J. G. Simmons, J. Appl. Phys. **41**(2), 545 (1970).
[3] J. C. Brenede, Z. K. Alaoui, N. Manai, Thin Solid Films, **235**,25 (1993).
[4] K. Gesheva, A. Szekeres, K. Gesheva Sol. Energy. Mat. Sol. Cells, **76**, 563 (2003).
[5] J. Zhou, N.-S. Xu, S.-Z. Deng, J. Chen, J.-C. She, and Z.-L. Wang, Adv. Mater. **15**(21), 835 (2003).
[6] J. N. Yao, K. Hascimoto, A. Fujishima, Nature, **355**, 624 (1992).
[7] R. Tokarz-Sobieraj, K. hermann, M. Witko, A. Blume, G. Mestl, R. Schlögl, Surface Science, **489**,107 (2001).

[8] A. Guerfi, L.H. Dao, J. Electrochem. Soc. **136** 2435 (1989).
[9] F. Hamelmann, K. Gesheva, T. Ivanova, A. Szekeres, M. Abrashev, and U. Heinzmann, J. Optoelectron. Adv. Mater. **7**(1), 393 (2005).
[10] N. Miyata, S. Akiyoshi, J. Appl. Phys. **58**(4), 1651 (1985).
[11] K. Gesheva, T. Ivanova, G. Popkirov, F. Hamelmann, J. Opt. Elect. Adv. Mater. **7**(1), 169 (2005).
[12] F. A. Chudnovskii, D. M. Schaefer, A. I. Gavrilyuk, R. Reifenberger, Appl. Sur. Sci. **62**, 145 (1992).
[13] P. I. Gouma, Rev. Adv. Mater. Sci. **5**, 147 (2003).
[14] M. Ferroni, V. Guidi, G. Martinelli, P. Nelli, M. Sacerdoti, and G. Sberveglieri, Thin Solid Films **307**, 148 (1997).
[15] A. R. James, S. Priya, K. Uchino, K. Srinivas, J. Appl. Phys. **90**(7), 3504 (2001).
[16] S. Lanfredi, J. F. Cravlho, A.C. Hemandes, J. Appl. Phys. **88**(1), 283. (2000).
[17] A. Huanosta, O. Alvarez-Fregoso, E. Amano, C. Tabares-Muňoz, M. E. Mendoza-Alvarez, J. G. Mendoza- Alvarez, J. Appl. Phys. **69**(1), 404 (1991).
[18] D. C. Sinclair, A. R. West, J. Appl. Phys. **66**(8), 3850 (1989).
[19] G. W. Bak, A. Szymanski, A. K. Jonscher, J. Chem. Faraday Trans. 2, **81**, 1053 (1985).
[20] K. Morii, H. Kawano, I. Fujii, T. Matsui, Y. Nakayama, J. Appl. Phys. J. Appl. Phys. **66**(8), 3850 (1989).
[21] R. Gerhardt, A. S. Nowick, J. Am. Ceram. Soc. **69**(9), 641(1986).
[22] L. K. Pan, H. T. Huang, C. Q. Sun, J. Appl. Phys. **94**(4), 2695 (2003).
[23] K. S. Cole, R. H. Cole, J. Chem. Phys. **9**, 341 (1941).
[24] J. Y. Zou, G. L. Schrader, Thin Solid Films, **324**, 52 (1998).
[25] D. Y. Wang, A. S. Nowick, J. Solid State Chem. **35**, 325 (1980).
[26] O. K. Varghese, L. K. Malhortra, J. Appl. Phys. **87**(10), 7457 (2000).
[27] M. El-Shabassy, A. S. Riad, Physica **B 222**, 153 (1996).
[28] K. K. Srivastava, A. Kumaro, O. S. Panwar, K. M. N. Lakshminarayan, J. Non-Cryst. Solids, **33**, 205 (1979).
[29] T. G. Abdel-Malik, M. E. Kassem, N. S. Aly, S. M. Khalil, Acta physica Polonica **A 81**(6), 675 (1992).
[30] K. Morii, H. Kawano, I. Fujii, T. Matsui, Y. Nakayama, J Appl. Phys. **78**(3), 1914 (1995).
[31] M. N. Kamalasanan, N. Deepak Kumar and S. Chandra, J. Appl. Phys. **74**(1), 679 (1993).
[32] Esmat Abdel Fattah I. Saad, Egypt. J. Solids, to be published.